The STAR Silicon Vertex Tracker:
A Large Area Silicon Drift Detector

R. Bellwied [f,1], R. Beuttenmuller [a], H. Caines [c], W. Chen [a],
D. DiMassimo [a], H. Dyke [c], D. Elliot [a], V. Eremin [a], M. Grau [a],
G. W. Hoffmann [e], T. Humanic [c], I. Ilyashenko [a], I. Kotov [c],
H. W. Kraner [a], P. Kuczewski [a], W.J. Leonhardt [a], Z. Li [a],
C. J. Liaw [a], G. LoCurto [c], D. Lynn [a], R. Minor [b], M. Munhoz [d],
G. Ott [a], S. U. Pandey [f], C. Pruneau [f], V. Rykov [f],
J. Schambach [c], J. Sedlmeir [a], B. Soja [a], E. Sugarbaker [c],
J. Takahashi [d], R. Willson [c]

[a]*Brookhaven National Laboratory*
[b]*Lawrence Berkeley National Laboratory*
[c]*Ohio State University*
[d]*University of Sao Paulo*
[e]*University of Texas, Austin*
[f]*Wayne State University*

Abstract

The STAR-SVT (Solenoidal Tracker At RHIC-Silicon Vertex Tracker) is a three barrel microvertex detector based upon silicon drift detector technology. As designed for the STAR-SVT, silicon drift detectors (SDDs) are capable of providing unambiguous two dimensional hit position measurements with resolutions on the order of 20 μm in each coordinate. In addition a high resolution energy loss measurement in the three layers of the SVT enables good particle identification. We describe features of the design of the STAR-SVT SDDs and electronics that are motivated by such characteristics. We also detail the mechanical structure, assembly procedures, and performance characteristics of the completed device.

[1] Corresponding author. Address: Brookhaven National Laboratory, Bldg. 510A, P.O. Box 5000, Upton, NY 11973. Email:bellwied@physics.wayne.edu

1 Introduction

The main purpose of the STAR Silicon Vertex Tracker (SVT) is to enhance the physics capabilities of the main STAR component, the STAR Time Projection Chamber (TPC). In addition to improving the primary vertexing, the two track separation resolution, and the energy-loss measurement for particle identification, the SVT also adds unique physics capabilities to STAR. It enables the reconstruction of very short-lived particles (primarily strange and multi-strange baryons and potentially D-mesons) through secondary vertexing close to the interaction zone. It also expands the kinematical acceptance for primary particles to very low momentum by using independent tracking in the SVT alone for charged particles that do not reach the active volume of the TPC due to the applied magnetic field.

In order to handle the expected high charge multiplicities (1500-3000 charged tracks per event) and to minimize the number of readout channels, silicon drift technology [1,2] was chosen. In this paper we give an overview of silicon drift detector technology, the specific STAR design, the electronics and mechanical components of the detector, and describe certain basic performance characteristics of the completed device. Further details of specific components can be found in series of recent STAR-SVT publications [3-20].

2 Characteristics of the STAR Silicon Drift Detectors(SDDs)

A silicon drift detector may be envisioned as a solid state time projection chamber. Highly homogenuous Neutron Transmutation Doped (NTD) 4in. n-type silicon wafers, produced by Wacker with a thickness of 280μm and a resistivity of 3 kΩcm, are used as starting material and several structures are implanted on each detector. p^+ strips (cathodes) are implanted symmetrically on both the top and bottom of the wafer and symmetrically biased with a potential having a gradient in the drift direction. We define the drift direction as $(\hat{X})$, the anode direction as $(\hat{Y})$, and the wafer thickness direction as $(\hat{Z})$. Segmented n^+ anodes are located at the edge of the detector and run in a direction parallel to the p^+ strips. A potential valley (as seen by an electron) is formed by the p^+/n junctions on both sides of the wafer such that ionized electrons generated by the passage of an energetic charged particle drift to the middle (in $\hat{Z}$) of the detector and towards the segmented anodes. The valley thus serves to constrain the electrons away from the surface of the detector to ensure full charge collection. Each STAR-SDD is 63 mm $\times$63 mm. It consist of a drift region (most of the detector area) and a focusing region (the last few millimeters before the anodes). In the focusing region an asymmetric potential is applied to the p^+ strips to focus the electron cloud towards the readout anodes. The current signal is then read through appropriate preamplifier electronics. The hit anodes determine the $\hat{Y}$ coordinate, and the drift time from the initial particle hit to readout of the signal determines the $\hat{X}$ coordinate.

The detector consists of two half-detectors separated by the dividing central cathode that receives the maximum voltage bias. Electrons in the half-detectors drift in opposite directions from one another. The main justification for the half-detector design is the need to limit the maximum drift voltage by limiting the maximum drift distance.

The anode design is driven by the requirement to achieve high resolution in the anode (or $\hat{Y}$) direction as well as the drift direction. In the anode direction the hit resolution is a function of the signal level, electronic noise, and level of charge sharing among adjacent anodes. The width of the charge diffusion determines the appropriate anode pitch to improve hit resolution through charge sharing. For drift times on the μs scale, expected charge widths are on the order of $\sigma \sim 100\mu m$ according to the diffusion equation $\sigma(t) = \sqrt{2Dt}$, where $D \approx 3.5\mu m^2/ns$ is the diffusion constant of electrons in silicon [21]. For charge depositions greater than a few MIPs (MIP = level of ionization for a mimimum ionizing particle) instant Coulomb repulsion results in widths greater than those calculated from the diffusion equation.

The segmented anodes are at a 250 μm pitch and are 200 μm $\times$ 200 μm in size. The pitch is appropriate over the range of signal gaussian widths ($70\mu m< \sigma < 200\mu m$) expected for drift distances between 1 mm and 3 cm and ionization from 1-10 MIPs. There are 240 anodes for each drift direction. The p$^+$ cathodes are implanted at a 135 μm pitch which maintains a suitably linear electric field in the bulk. Adjacent cathodes are connected via 'M' shaped implanted resistors at the edge of the cathodes. The guard strips (p$^+$ implants with aluminum overlay) that connect to every 10th cathode serve two purposes. First, each 10th cathode of one half-detector connects to that of the other half detector; thus only one half-detector requires external bias and the other half is automatically biased. Second, the guard strips provide a controlled voltage step-down gradient between the high voltage implants near the center of the detector (i.e. the continental divide) and the cut edge of the detector. This is necessary to prevent electric breakdown in this region where the voltage gradients on the detector are the greatest. Considerable effort was devoted to minimizing the guard area, resulting in design with a 94.5% active area. There are a total on 220 cathodes on each half-detector, and one common center cathode (i.e. the continental divide). Externally biasing each of these cathodes via wirebonds, while possible, would significantly increase the complexity of the wire bonding and the mechanical support. The chosen design in which only every 10th cathode is wire bonded resulted in a considerable reduction in the number of wire bonds. This, however, necessitated having an internal on-detector resistor chain to bias the cathodes between every 10th bond. The values of the internal resistors were chosen to be 500 kΩ. These values were sufficiently large to minimize power dissipation and thus temperature gradients below 0.3°C. Together with a sufficiently stiff external voltage divider (15 kΩ between every 10th cathode) the resistor chain maintains the necessary uniformity in the electric field to permit $20\mu m$ position resolution.

The primary challenge of silicon drift detectors is to achieve and maintain the best possible hit resolution in the drift direction, which depends upon maintaining a

3

highly linear drift velocity across the detector. The drift velocity is a function of the silicon temperature, the applied electric field, and the applied magnetic field. The requirement of stabilizing the detector performance against variation of these quantities has implications on the detector design which are detailed in [4,16]. In addition, four MOS(Metal-Oxide-Semiconductor) injection lines per half detector provide online drift velocity calibration and are described in [12].

The electron drift velocity v_e is given by $v_e = \mu_e E$, where μ_e is the electron mobility in silicon and E is the applied electric field. The electric field is usually limited to less than 1000 V/cm, below which the electron mobility is independent of E and is equal to 1350 cm^2/Vs at 300K [22].

The nominal working voltage of the STAR SDD is -1500 volts. Since each half detector has a drift distance of approximately 3cm, this results in an electric field $E = 500$V/cm. The drift velocity then amounts to 6.75μm/ns, and the corresponding maximum drift time $t_{drift} \approx 4.5\mu$s

Fig. 1 shows linearity measurements made on a STAR SDD using a laser mounted on a precision coordinate table. An injected signal of approximately 10 MIPs was used to eliminate noise influences in the measurements. Fig. 1a shows measurements of drift distance vs. drift time which appear highly linear. Measurements were made in 100μm steps along the drift coordinate. Fig. 1b shows the difference between a fit line and the data shown in Fig. 1a. Two distinct slopes are seen that correspond to the focusing and the drift regions of the detector. Fig. 1c shows a histogram of the deviation of those data points in the drift region from a fit line. An rms of 17μm is obtained. Similar rms values are obtained across all anodes in a detector, though the slopes of the fit line vary from the center anode to the edge anodes due to the thermal gradients produced by the current flow through the implanted resistors. A similar measurement was made in the anode direction and an rms of 8μm was obtained as seen in Fig. 1d.

In order to account for drift time variations (both temperature-gradient induced and intrinsic) to obtain maximum hit resolution, the drift profile of each detector mounted on a ladder is measured by scanning a laser across the detector at various drift distances prior to installation in the SVT. The mapping of the detectors is performed under similar environmental conditions of air and water cooling as provided in the installed SVT and subsequently entered into a database for use in the calibration and analysis of the SVT data. Under running conditions, small changes in the drift velocity due to deviations in the absolute detector temperature are monitored with the detector injectors. These provide a single correction factor for each detector for changes in the mean drift velocity. The final SVT system test with the cooling system decribed in one of the following section showed that this correction is unnecessary under normal running conditions, as the temperature changes resulted in drift coordinate deviations of at most 5μm rms once the ladder had reached its mean operating temperature. These deviations were measured over a two hour period after a two hour detector burn-in period following the initial power-up. The above linearity measurements yield the intrinsic resolutions of the SDDs. To obtain hit position resolutions, these measurements were repeated with single MIP laser
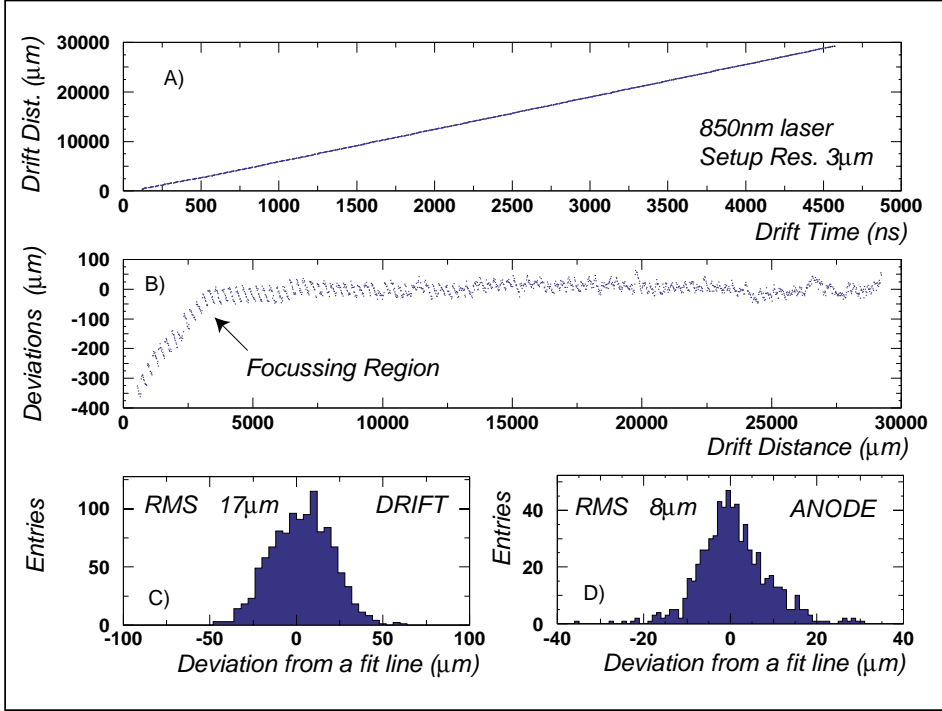
Fig. 1. A)Laser measurement of drift time vs. drift distance on a SVT SDD in a system test. B) Difference between data points in drift region and a straight line fit. C) Histogram of difference between data points and straight line. D) Histogram of difference between actual and reconstructed position of laser injection hit in anode direction.

injection, taking one measurement at each 100μm step in the drift direction. Thus these measurements include the effects of electronic noise (ENC = 530 e- rms as described in the following section) and detector drift non-linearities. Typical position resolution values obtained across the detector were 20μm and 25μm in the anode and drift directions, respectively.

In addition to the position resolution, the detector also yields an energy measurement on the basis of the charged particle energy loss (dE/dx) in each layer. Fig. 2 shows an actual measurement from an array of STAR-SDD's in a 11.6 A Gev/c central Au-Au collision at the BNL-AGS. Based on these results we estimate the dE/dx resolution of the STAR-SVT to be about 7%.

In summary, during the research and development phase of SVT project (1993-1996), around 200 wafers of various designs were produced at BNL [18,19]. Commercial production of the wafers based on the final design was awarded to SINTEF, a Norwegian company that subsequently produced 350 wafers over a period of two years. The production yield was slightly above 70%. The quality control criteria and testing procedures are detailed in [7,9].
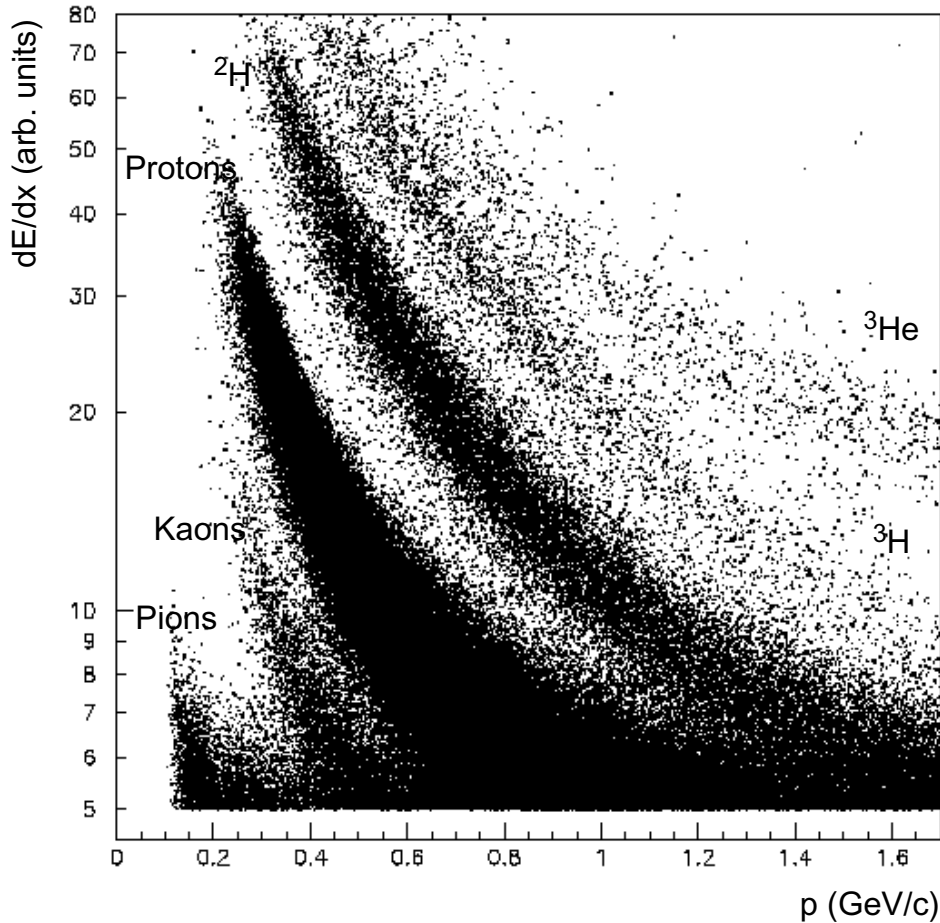
Fig. 2. dE/dx measurement from fixed target Au-Au collisions at 11.6 GeV/n using an array of STAR-SDD's

3 Front-end Multi-Chip Module Electronics

The primary purpose of the front-end electronics is to amplify and shape the detector current signal arriving via the detector anodes such that time-of-arrival and total charge information are preserved. The front-end must also minimize the noise introduced into these measurements. A photograph of the STAR-SVT front-end multi-chip module(MCM) is shown in Fig. 3. We will only discuss in general terms the MCM design as a detailed discussion may be found in [5].

A feature of drift detectors is their small anode capacitance (typically < 500 fF). This is the result of the small geometric size of the anode and the depletion of the silicon bulk. In order not to significantly increase this input capacitance, the interconnect between the anode and the front-end transistor should be no longer than approximately 1 cm (a general rule-of-thumb gives 1pF/cm for a variety of interconnects, e.g. bond wires, printed circuit signal traces).

Fig. 3 shows a row of 240 input pads that are spaced at the detector anode pitch of
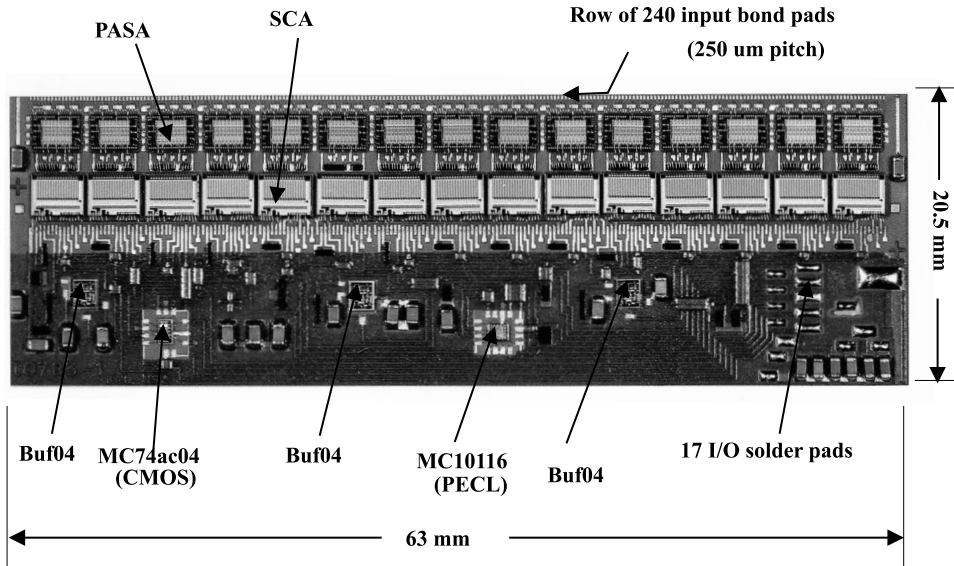
SVT Front End Hybrid/MCM

Fig. 3. SVT Front-end Multi-Chip Module

250 μm and that are intended to be wire bonded to the SDD anodes. Each of these pads has a second wire bond to an input pad of the PreAmplifer ShAper (PASA) die. Measurements indicate that each of these bond wires contribute about 170 e- (electrons) rms noise, which is only about an additional 30 e- rms when added in quadrature to the other noise sources.

The low input capacitance permits a fast preamplifier-shaper response due to the lower series (capacitance dependent) noise. A fast impulse response is desirable for good separation of charge from two hits arriving on the same anode(two-track resolution). 'Fast' is therefore defined relative to the expected separations and widths of adjacent hits and in the case of the SVT refers to a risetime (10-100%) of 50 ns. The PASA was thus implemented in bipolar technology rather than CMOS based on its superior noise-power performance at such clocking speeds. A bipolar signal shape also helps to avoid baseline shifts due to the high hit multiplicity in the heavy ion environment. Characteristics of the 16 channel PASA are listed in Fig. 4.

It is necessary to have waveform sampling to preserve both timing and dE/dx information. The number of required samples is determined by $N \times 1/f_{sampling} > t_{drift}$, where N is the number of samples, $f_{sampling}$ is the sampling frequency, and t_{drift} the total SDD drift time. In order to avoid corruption of the output waveform the sampling frequency should be greater than twice the PASA bandwidth of about 10 MHz. We chose $f_{sampling} \approx 25$MHz, which together with the drift time of about 4.5μs suggests that the number of samples be greater than 112. The front-end is thus designed for 128 samples which, as a power of two, is naturally implemented.

In order to reduce the number of output channels per MCM (nominally 240), it is desirable to have a level of multiplexing at the MCM. Due to the waveform sampling, however, there are $128 \times 240 = 30,720$ pixels per half-detector or MCM.

7

FEE Parameters and Specifications

Multi-Chip Module	
Technology	Thick Film on beryllia substrate
	Dupont QM silver based pastes
Size	63 mm x 20.5 mm
No. Channels	240
No. Time Samples	128/channel
Total No. "pixels"	128 x 240=30,720
Output channels	3 (for 10,240 pixels)
Sampling Rate	25 Mhz
Readout Rate	2MHz
	10,240/2MHz = 5 ms
Power Dissipation	12 mW/Channel = 2.9 W
Noise	ENC = 490 e- rms (no detector)
	ENC = 530 e- rms (w/ biased detector)
Radiation Length	1.4%

PASA	
Technology	Maxim SHPi NPN-BJT process
Die Size	3.3 mm x 2.4 mm
No. Channels	16
Power Dissipation	3.8 mW/Channel
Gain	7.2 uV/e-
Noise (C_{in} < 0.2 pF)	ENC = 380 e-
Peaking Time (10-100%)	50 ns
Dynamic Range	2 V (275,000 e-)

SCA	
Technology	Orbit 1.2 um CMOS
Die Size	3.8 mm x 2.8 mm
No. Channels	16
No. Capacitor/Channel	128
Power Dissipation	6 mW/Channel
Noise (C_{in} < 0.2 pF)	2.2 mV (ENC = 300 e- rms)

Fig. 4. FEE Parameters and Specifications

A solution involving front-end digitization before multiplexing is prohibitive due to the large number of pixels. An analog multiplexing scheme is required and is implemented with Switched Capacitor Array (SCA) integrated circuits [23]. Detailed specifications of the SCA are given in Fig. 4.

Each SCA is operated as a circular memory buffer. The output PASA waveform is sequentially sampled on each of the 128 capacitors on a given SCA channel. After 128 capacitors have been written, an internal counter resets and sampling continues, overwriting previous values. The SCA and thus the detector is continuously active until a trigger is received and readout of the SCAs begins. The signals on all $128 \times 16 = 2048$ capacitors per SCA are multiplexed onto one common analog output. An arbitrary number of SCAs may be multiplexed together. In the implementation chosen for the SVT, groups of five SCAs (80 channels or 10,240 pixels) are multiplexed. Therefore there are three analog outputs per MCM. Analog Devices' Buf04 analog drivers (see Fig. 3) were used to drive the output. A commercial CMOS chip for the SCA control circuitry and an ECL chip for the differential clock to the SCA are also shown in Fig. 3. The main specifications of the MCM are summarized in Fig. 4.

4 Ladder Components

The optimization of the resolutions achievable with the complete STAR detector requires the minimization of materials within the active volume of the detector. To satisfy this constraint, the SDDs and related components were assembled onto support elements where most of the material is cut away giving the structures a shape similar to ordinary ladders.

The very compact layout of the SVT required the ladder design to follow as closely

as possible a dense polygon shape. Thus, the necessary frontend electronics modules had to be arranged at an angle with respect to the detectors. This angle changes according to the barrel radius from 22.5^o to 30° to 45°, respectively. Each SVT ladder therefore consists of three mechanical components: a detector carrier and two electronics carriers (ECs). These three components are connected via angle brackets made of G-10. During the wirebonding of the electronics to the detector anodes, all three components are in-plane. After completion of the bonding the two electronics carriers were lowered onto the angle brackets and screwed in place. The ECs were made from graphite epoxy material and their outside dimensions are 20 mm wide by 1.8 mm thick by a length to match the length of their respective DC. Further, the ECs are hollow, providing an internal water cooling channel 13.9 mm wide by 1 mm high. The ECs have the MCM mounted on their upper surface and additional circuitry mounted on their lower surface.

The detector carriers are made from 1.8mm thick beryllium that is 63mm wide by the ladder length. Two different lengths of DCs are used (530 and 560mm) resulting in two different lengths of ladders. These two lengths are necessary to allow 'nesting' of the ladder assemblies and, thus, a more compact detector. The SDDs are attached to the DCs by placing them in lines of epoxy adhesive laid down along the DC edges. The epoxy contained precision balls to ensure the SDDs were placed in plane.

Fig. 5 shows the main components of one complete ladder of detectors and electronics. Thirty six such ladders (with either seven, six, or four detectors) arranged in three barrels constitute the full SVT. The ladder in the figure contains seven SDDs. The two outermost detectors are bonded to High Voltage Interface boards (HVI). Each HVI supplies the approximately 30 voltages needed to bias the SDDs. These voltages are derived from a stiff voltage divider located on the Transition Board, which resides on the SVT water manifold at a distance of about 15 cm. The board is connected to the HVI via a small gauge HV cable capable of withstanding over 12kV. The stiff divider is located away from the detector in order to avoid coupling its 7.5 watts power dissipation into the detectors and introducing drift non-linearities. The HV input of the left and right side of each ladder is decoupled in order to avoid large ground loops. Thus all the half-ladders, including their associated electronics, are electrically isolated from each other.

Thin printed circuit cables (PCCs) are epoxied to the underside of the electronics carrier. These cables contain digital differential receivers which receive and drive the clock and control signals to operate the SCAs. They connect to each MCM via a custom fabricated 'wrap-around' cable made of small gauge magnet wire. The wrap-around cables connect the MCM input/output with the PCC. The analog outputs from each MCM are driven single-ended through the PCC and via the Low Voltage cable to the transition board, where, in addition to the external detector voltage divider, analog differential drivers are located. These drivers convert the single-ended analog signals to differential levels and drive the signals via shielded twisted-pair cable a distance of about 10 feet to the readout system where the signals are digitized.
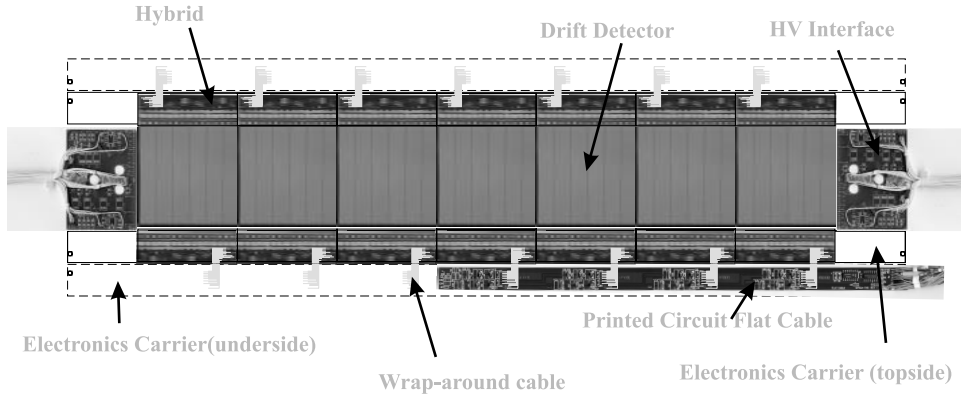
Detector Ladder Components

Fig. 5. Components comprising one of 36 STAR-SVT ladder assemblies

5 Readout Electronics

The main readout electronics functions are to acquire and digitize analog data, add header information, transfer data to DAQ via Gigalink Fiber, control system parameters via slow control, monitor voltages and temperatures, supply and switch hybrid power, supply hybrid controls and clocks, and control the input into the charge injector lines.

On the TPC wheel 24 SVT readout electronics (RDO) boxes are mounted, twelve on each side of STAR. Each RDO box has 54 analog inputs. Data acquisition is performed at 8/3 of the RHIC strobe frequency (25MHz). Digitization occurs at 60/36 of the fiber link frequency of 60MHz (1.67MHz). The total duration of digitization and fiber optic transfer is about 7.3ms.

The RDO system is split into 3 functional blocks: a monitoring, power, trigger and slow control interface block (PTB), an analog to digital converter and data storage block (AMB), and a fiber optic transfer block (FOB). These blocks are implemented on VME 6U-size boards, connected via VME-like back planes. Due to connector space constraints, the analog part is distributed over five AMB boards and the monitor, power and trigger interfaces are split amongst 2 PTB boards and a front panel, which means each RDO box hosts up to eight boards. Each RDO box connects to three transition boards, located on the water manifold close to the detector, which in turn connect to three ladders. Each transition board (2 by 18 cm) hosts the external resistor (voltage divider) chain for the specific ladder it is connected to. Each RDO box is equipped with standard STAR Trigger, DAQ and slow controls interfaces. The RDO system components are cooled by connecting each RDO box into the TPC chilled water system.

6 Support Structure

The SVT consists of a total of 216 SDDs arranged in three barrels around the beampipe at radii of approximately 6.9cm, 10.8cm, and 14.5cm from the intersection point. Each barrel consists of a set of ladders comprised of four, six, and seven wafers per ladder, respectively. The barrels consist of eight, twelve, and sixteen ladders, respectively.

The active Silicon length in beam direction is 25.2 cm for the inner barrel, 37.8 cm for the middle barrel and 44.4 cm for the outer barrel. Each detector carrier (incl. wafers) contributes 0.35% radiation length, and each electronics carrier (incl. electronics and filled with water) contributes 2.37% radiation length to the total thickness. The total averaged radiation length of the SVT is a little below 6% for all three layers or 1.89% per layer.

Each ladder of the SVT is mounted in two edge locations onto the SVT beryllium end rings. Each detector side has two endrings, an inner and an outer one. Barrel one is supported by the inner endrings, barrels two and three are mounted to the inside and the outside of the outer end rings, respectively. The endring thickness is 1mm and each end ring consists of two halves, which enables the assembly of the SVT into two halfshells in order to install the detector without breaking the vacuum in the RHIC beam pipe.

The SVT surrounds the primary interaction point in STAR. It resides inside the TPC inner field cage and thus can only be supported from outside the TPC itself. From each TPC endwheel a cone structure reaches into the area between the interaction point and the TPC inner field cage in order to support the SVT. These cones are made of an ultralight honeycomb structure composed of graphite-epoxy (0.64% radiation length). Cables and water lines are mounted to the outside of the cone and connect the components on the TPC wheel to the components on the detector and the water manifold. A smooth cone surface is necessary to avoid sparking from the TPC inner field cage to the SVT. The system is laid out for a maximum voltage of 80 kV on the TPC. Thus the cable and water line layer was enclosed with a smooth fiberglass shell of 1 mm thickness. The cones themselves are conical only out to a distance of 1.5 m from the intersection point. Here they transition into a cylindrical shape up to the TPC wheel in order to allow installation of the STAR forward TPC's into the STAR solenoid. Aluminized Mylar sheets of varying thickness (from 75 to 125 micron) have been used to surround the SVT and electrically shield it.

The two cones are connected through two elliptical honeycomb rods located at a radius slightly larger than the outermost layer of the SVT in the 12 and 6 o'clock positions, respectively. The cones are only supported at the TPC wheels, about 2 m from the center point of STAR. Alignment adjusters are located at the TPC wheel and the water manifold, in order to adjust the positioning of the SVT with respect to the TPC.

Figs. 6 and 7 show photographs of the final SVT on the cone support just before

Fig. 6. The final SVT just before installation of the second half-shell installation into the TPC.

7 Conventional Systems

The conventional systems part of the SVT consists of an air cooling system that supplies air to the SVT and TPC volume inside the TPC inner field cage, and a water system that pumps water through the electronics carriers of each SVT ladder.

The air system is an open system which takes air from the room, conditions it, and then flows it through the SVT and the inner field cage of the TPC. It is then discharged back into the room. The system uses fans, a heater, a cooler and a HEPA filter to supply clean air at a constant temperature of about 23°C and around 50% relative humidity. The system removes about 180 W of heat from the SVT volume, mostly generated by the SDDs as well as nearby cables and circuit boards. The air flow is continuous and always slightly above the required 3400 liter/min.

The water system, on the other hand, is a closed loop system. The system contains a pump, filter, heat exchanger and heater and flows about 40 liter/min. of water through the SVT to remove about 1.6kW of heat and limit the temperature rise of the water to about 1° C. A vacuum pump is used in conjunction with the water system to lower the overall pressure of the system such that the absolute pressure inside the STAR detector is below atmospheric pressure. This is known as a leakless system since, if a leak occurs, the system will pull air rather than leak water. This
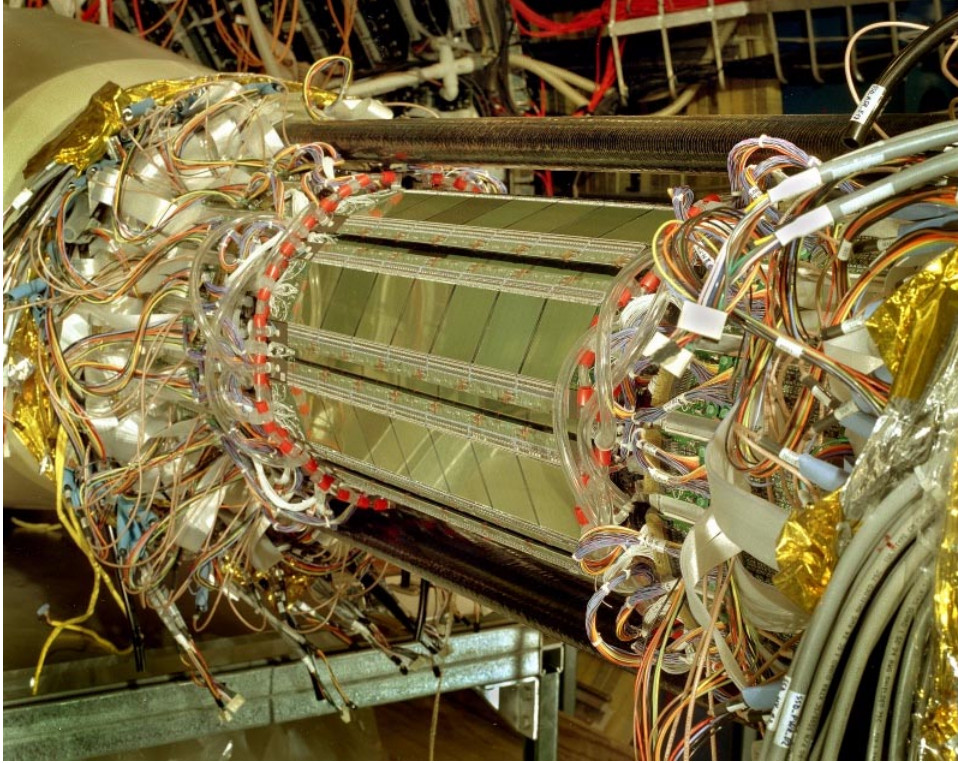
Fig. 7. The final SVT on the support cone

air is removed by the vacuum pump.

Water is pulled through the system from the water pump to a manifold located on the TPC wheel on the detector east side. From there 10 water lines run down the cone to the SVT water manifolds located close to the detector itself. These manifold have a polygonial shape with 18 sides. An electronics transition board is mounted to each inside and outside face of both manifolds (total of 72 boards). From the first manifold, water is distributed to every electronics carrier, which means the ten water manifold inlets are fanned out to 72 water manifold outlets. After traversing the electronics carriers, the water is then collected in the same way in the second water manifold, and pumped back to the water reservoir. Each water manifold is made of aluminum and has an inner radius of 15.1 cm and an outer radius of 16.8 cm. Its length in beam direction is 18.1 cm, starting at a distance of 33.4 cm from the intersection point on each side of the SVT.

8 Summary

The STAR Silicon Vertex Tracker is a microvertex detector implemented in the novel silicon drift detector technology. Drift detectors permit high resolution unambiguous two-dimensional hit position measurements with readout of only one edge of the silicon wafer. The SVT consists of 216 SDDs containing over 13 million pixels multiplexed onto just 1300 readout channels. A 'pixel' in a drift detector is defined

by the anode segmentation in one coordinate and the drift velocity divided by the sampling frequency in the drift direction coordinate. The pixel-like readout of the silicon drift detector makes it a good choice for the high multiplicity environment in heavy ion reactions at RHIC. In this case, however, to avoid hits in the detector from interactions separated in time, the interaction rate should be much less than $1/t_{drift} \sim 100\text{kHz}$. For lower multiplicity interactions (proton-proton, for example), this constraint may be eased as the lower multiplicities may permit proper association of the hit to its initial beam interaction.

Position resolutions of $20\mu m$ in both coordinates as well as energy loss (dE/dx) measurements with a resolution of about 7% were achieved with the STAR-SVT. Based on the successful completion of the STAR-SVT one can conclude that Silicon drift detectors are a competitive technology for small vertexing detectors (based on performance characteristics) as well as large area tracking detectors (based on performance and cost).

The full SVT has been completed and the detector system has been installed in STAR in time for data acquisition during the RHIC 2001 run.

9   Acknowledgements

References

[1] E. Gatti and P. Rehak, *Nucl. Instr. and Meth.* **225**, (1984) 608.

[2] W. Chen et al., *IEEE Trans. Nucl. Sci.* **41** (1994) 941

[3] J. Takahashi et al. (SVT Coll.), *Nucl. Instr. and Meth.* **A453** (2000) 131.

[4] D. Lynn et al. (SVT Coll.), *Nucl. Instr. and Meth.* **A447** (2000) 264

[5] D. Lynn et al. (SVT Coll.), *Nucl. Instr. and Meth.* **A439** (2000) 418

[6] R. Bellwied et.al. (SVT Coll.), *Nucl. Inst. and Meth.* **A439** (2000) 507

[7] J. Takahashi et al. (SVT Coll.), *Nucl. Inst. and Meth.* **A439** (2000) 497

[8] J. Takahashi et al. (SVT Coll.), *IEEE Trans. Nucl. Sci.* **47** (2000) 903

[9] A. Asmus et al. (SVT Coll.), *IEEE Trans. Nucl. Sci.* **47** (2000) 1375

[10] S. Pandey et al. (SVT Coll.), *Nucl. Phys.* **A661** (1999) 686c

[11] R. Bellwied et al. (SVT Coll.), *IEEE Trans. Nucl. Sci.* **46** (1999) 176

[12] R. Bellwied et al. (SVT Coll.), .*Nucl. Instr. and Meth.* **A416** (1998) 70

[13] R. Bellwied et al. (SVT Coll.), *IEEE Trans. Nucl. Sci.* **45** (1998) 623

[14] S. Pandey et al. (SVT Coll.), *IEEE Trans. Nucl. Sci.* **45** (1998) 315

[15] R. Bellwied et al. (SVT Coll.), *Nucl. Instr. and Meth.* **A416** (1998) 70.

[16] S. Pandey et al. (SVT Coll.),*IEEE Trans. Nucl. Sci.* **44** (1997) 610

[17] R. Bellwied et al. (SVT Coll.), *IEEE Trans. Nucl. Sci.* **44** (1997) 687

[18] R. Bellwied et al. (SVT Coll.), *Nucl. Inst. and Meth.* **A400** (1997) 279

[19] R. Bellwied et al. (SVT Coll.), *Nucl. Instr. and Meth.* **A377** (1996) 387.

[20] S. Pandey et al. (SVT Coll.), *Nucl. Instr. and Meth.* **A383** (1996) 537.

[21] E. Gatti and P.F. Manfredi.,*Revista Nuovo Cimento* **9**, 1 (1986)

[22] W.R. Leo, Techniques for Nuclear and Particle Experiments, 2nd Ed., (Springer-Verlag, Berlin, 1994)

[23] S.A. Kleinfelder *IEEE Trans. on Nucl. Science* **37** (1990) 1230